7. EXPERIMENTAL VALIDATION OF THE EFFECT OF BRAKING TORQUE TO BOGIE DYNAMICS: PART B. EXPERIMENTAL RESULTS

7.1. INTRODUCTION

This chapter reports some important results of the experiment presented in Chapter 6. Three cases of the bogie brake dynamics experiments were selected as listed in Table 7.1. For each case brake application time was set as 0.8 sec.

Table 7.1. Cases of the experiment

Case	Brake Pressure (kPa)
Case #1	130 kPa
Case #2	150 kPa
Case #3	180 kPa

Of the three cases examined, Case #2 (150 kPa pressure) was considered to be just on the verge of the onset of skid; any increase in pressure above this level was expected to most certainly induce skid (based on simple analytical calculation). Brake pressures of Case #1 and Case #3, could therefore be regarded as cases of mild (no possible skid) and heavy (high possibly skid) braking respectively.

This chapter describes the primary and derived data obtained from each case of the experimental program.

The primary data included:

1. Brake normal forces (kN); measured by the strain gauge on the brake rod
2. Tangential brake forces (kN); measured by the strain gauge on the brake beam hanger
3. Accelerations (m/s^2) in the longitudinal, the lateral and the vertical directions; measured by the accelerometers
4. Linear distance travelled (m); measured by the LIMES linear encoder
5. Angular revolution (rad); measured by the HENGSTLER shaft encoders

The derived data included:

1. Brake torque; calculated from the tangential brake force
2. Longitudinal speed profile (m/s); first derivative of the LIMES data
3. Angular velocity (rad/s); first derivative of the HENGSTLER data
4. Longitudinal acceleration (m/s^2); second derivative of the LIMES data
5. Slip

Where possible the derived data were compared to the measured primary data.

7.2. EXPERIMENT CASE #1 (P=130 KPA)

Four trials were executed where the brake cylinder pressure was set up to achieve 130 kPa within 0.8 second.

7.2.1. Primary Data

Brake cylinder forces – normal and tangential

The brake cylinder forces in the normal and in the tangential direction to the wheel tread at the point of application were measured using the strain gauged brake rods and brake beam hangers respectively. Fig. 7.1 presents the brake cylinder pressure and forces measured in the brake rods of each cylinder for trial 1 to trial 4. As can be seen in the figure, the pressure in the brake cylinder increased gradually from zero to 130 kPa in 0.8 second. The forces in the brake rods also increased gradually from zero to maximum during the corresponding period without any time lag. Both rods measured approximately the same magnitude of brake shoe normal forces. Using the specification of the new bogie (0.164 kN total normal force per kPa, see Section 6.2), the force in the rods was calculated as 5.33 kN, which was approximately 18% higher than the measurement. As the bogie was a refurbished old one, it was expected that lower efficiency of the cylinder would exist; the 18% reduction was, therefore, acceptable.

Fig. 7.2 shows the tangential brake force measured from the brake beam hanger for trials 1 to 4. Tangential brake force can be calculated as a function of the brake shoe normal force: $F_T = F_B \mu_b$, where μ_b is the friction coefficient between brake shoe and wheel tread and F_T and F_B are tangential and normal brake shoe force respectively (see Section 2.5). As both the normal and the tangential brake shoe forces were measured, the friction coefficient between the brake shoe and the wheel tread (μ_s) was able to be calculated; the calculated values varied between 0.27 and 0.33.

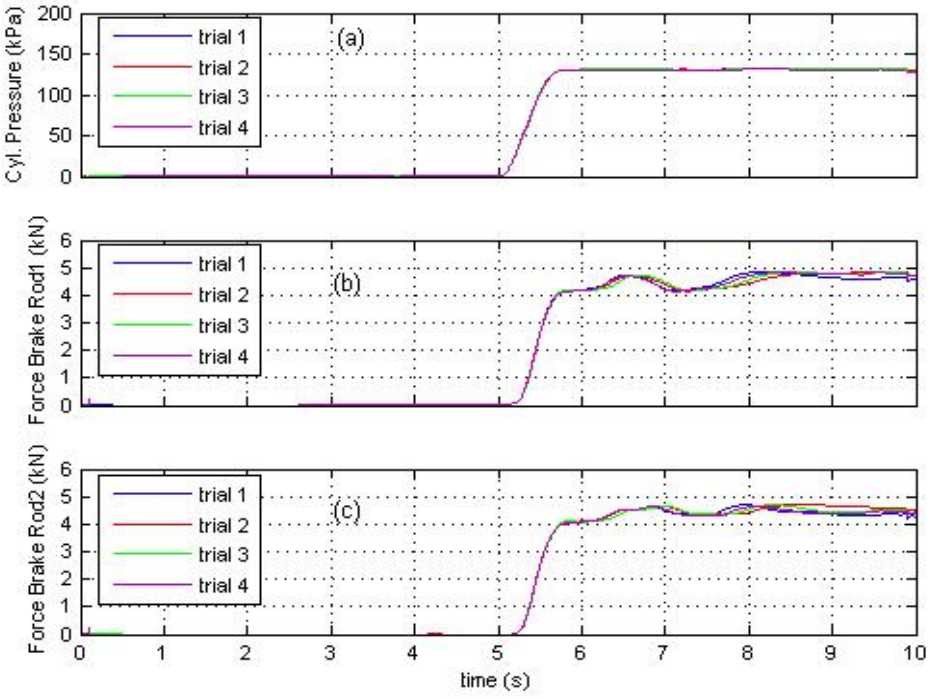

Figure 7.1. Brake cylinder pressure and normal forces in the brake rods, Case #1

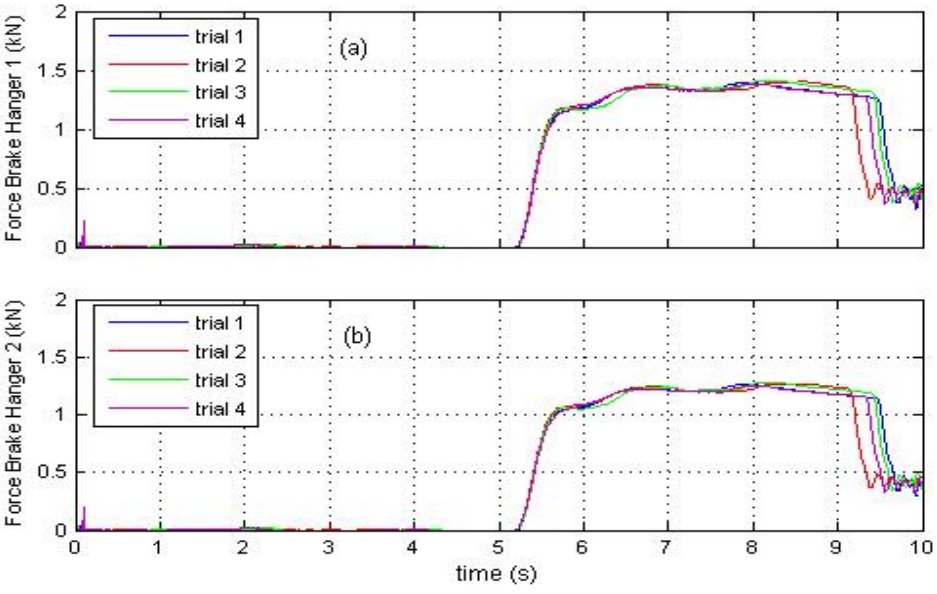

Figure 7.2. Tangential brake force in the brake beam hangers, Case #1

Acceleration – longitudinal, lateral and vertical

During the experiment, the longitudinal, the lateral and the vertical accelerations were measured using the accelerometers fitted to the axle boxes (see Section 6.2 and Section 6.3). Fig. 7.3 shows the average of the measured longitudinal acceleration obtained from four accelerometers which show very good consistency amongst the four trials although each trial was conducted *without* any assurance of repeatability. The maximum longitudinal acceleration recorded varied from 2.4 m/s^2 to 2.8 m/s^2, which is considered not very significant (16% variation). In the coasting zone each trial has provided very consistent acceleration (a deceleration of approximately 0.1 m/s^2). In the braking zone (the zone of interest of this test program) where the controlled brake was applied, the deceleration obtained from each trial remained relatively the same (approximately 0.75 m/s^2). Therefore the cost-effective means of accelerating the bogie was considered technically sound and satisfactory for the purpose of the investigation.

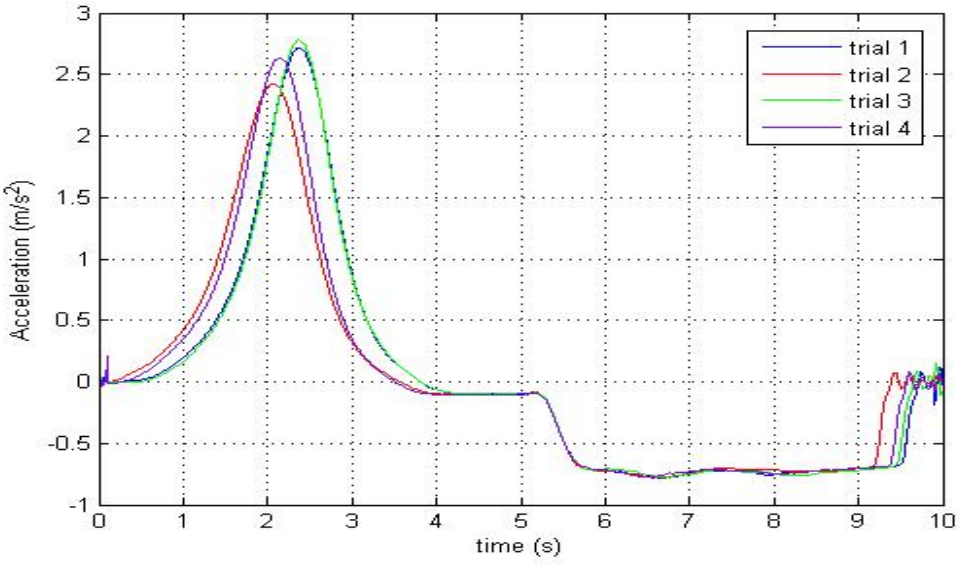

Figure 7.3. Longitudinal accelerations measured by accelerometers, Case #1

Fig.7.4 and Fig.7.5 show, respectively, the lateral (average of two measurements) and the vertical (average of four measurements) accelerations measured using the accelerometers. The magnitude of these accelerations was very small both in absolute term and relative to the longitudinal acceleration (Fig.7.3). The low magnitude could be regarded as an indication of the good control exercised in each trial especially the precision of the applied pull without any lateral shift; it also reflected on the smoothness of the track, in particular the top surface of the rail. The lateral and the vertical accelerations remained negligibly small for *all three cases* of the experiment reported in this chapter; thus these are not presented for other cases. All cases of the experiment can, therefore, be regarded as pure longitudinal dynamics investigation.

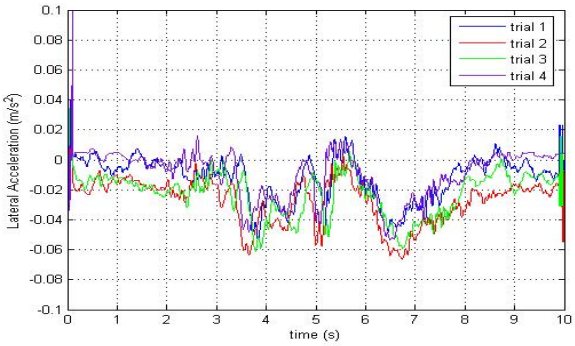

Figure 7.4. Lateral accelerations measured by accelerometers, Case #1

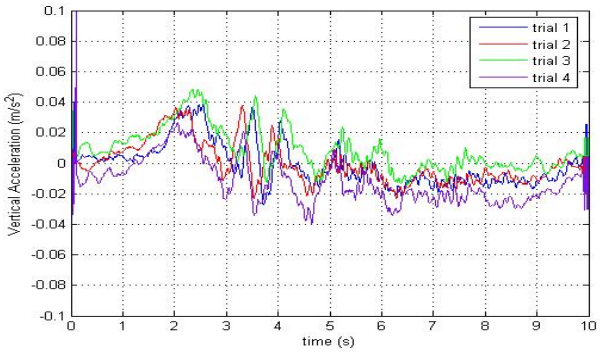

Figure 7.5. Vertical accelerations measured by accelerometers, Case #1

Linear distance travelled and angular revolution of wheelsets

The linear distance travelled of the bogie along the test track is shown in Fig.7.6.c, while the angular revolution of the leading and the trailing wheelsets are respectively presented in Fig.7.6.a and b. This figure depicts that the longest travel distance was approximately 16 m. During this travel, the wheelsets rotated approximately 40 rad, or just more than six full rotations.

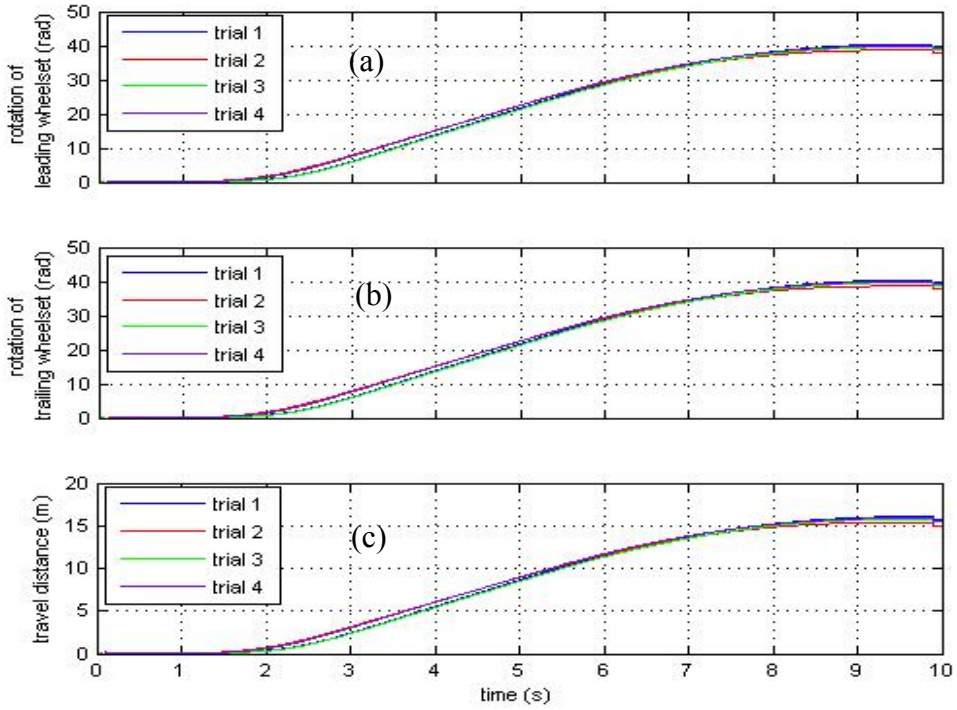

Figure 7.6. Travel distance and rotation of wheelsets, Case #1

7.2.2. Derived Data

Brake torque

Brake torque applied to the trailing wheelset was calculated using Eq.(7.1):

$$T_B = \left(F_{T1} + F_{T2}\right) r_w \qquad (7.1)$$

where T_B denotes the brake torque, F_{T1} and F_{T2} are the tangential force measured in hangers 1 and 2 respectively and r_w is the nominal radius of the wheels (0.398 m, measured before the test). The calculated brake torque time series is shown in the Fig. 7.7.

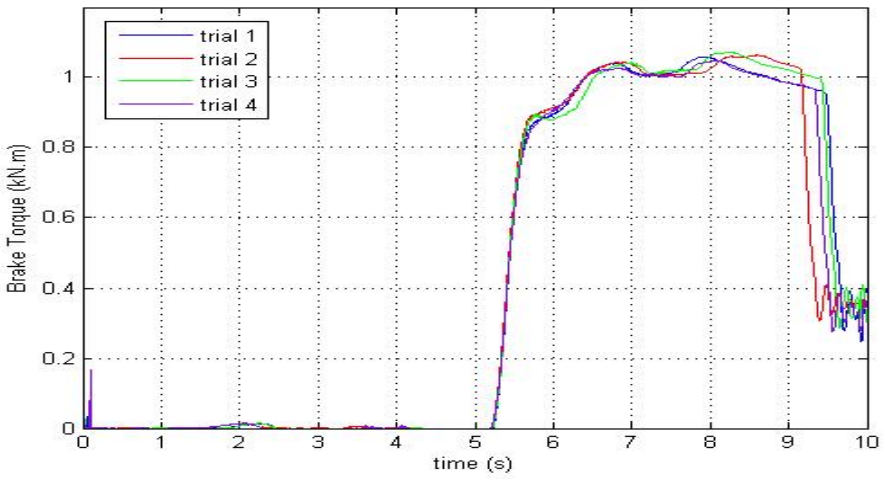

Figure 7.7. Brake torques applied to the trailing wheelset, Case #1

Speed profile and angular velocity of the wheelset

Fig. 7.8 shows the bogie speed profile and the angular velocities of the wheelsets. The bogie speed profile is the first derivative of the dataset obtained by the LIMES linear encoder with respect to time whilst the angular velocities of the wheelsets were obtained from the first derivatives of the HENGSTLER shaft encoder datasets. From Fig. 7.8, we can see that no skid happened at the braked trailing wheelset for all four trials as its angular velocity was reduced to zero at the same rate as the bogie speed and the angular velocity of the non braked leading wheelset. The maximum speed obtained was 3.14 m/s (trial 1), which was lower than the 4 m/s maximum speed for which the experiment was designed (Chapter 6). With the nominal wheel radius of 0.398 mm

(measured), the maximum angular velocity of 7.89 rad/s was calculated. The measured maximum angular velocity was 7.90 rad/s, showing the precision of the measurement system.

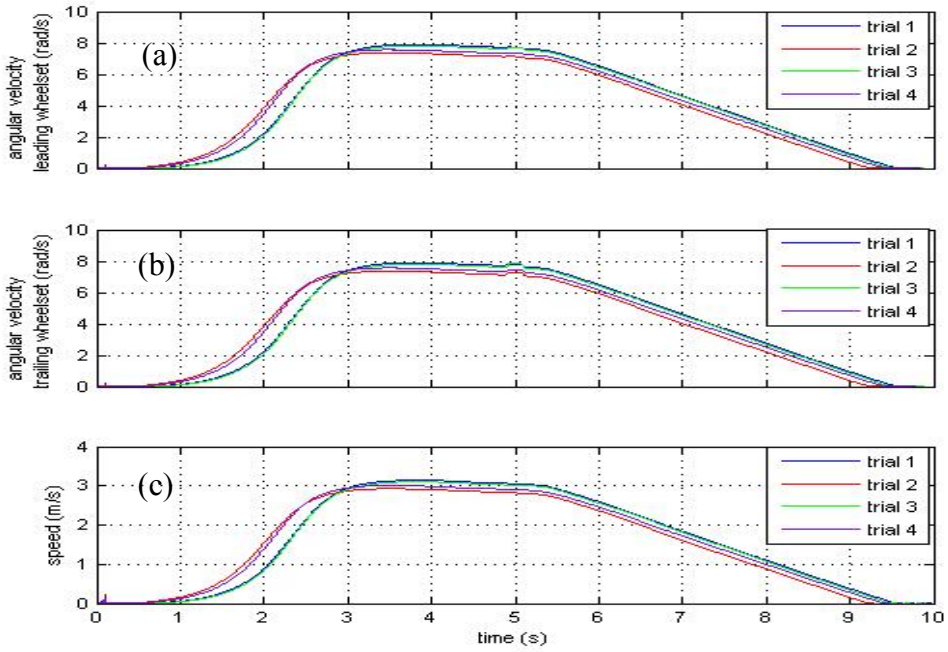

Figure 7.8. Speed profile and wheelsets angular velocity, Case 1

Longitudinal accelerations

Fig. 7.9 exhibits the bogie longitudinal acceleration calculated through the second order numerical differentiation of the linear distance data obtained from the LIMES linear encoder. It provides a very good agreement with the direct measurement of longitudinal acceleration using accelerometers (Fig. 7.3)

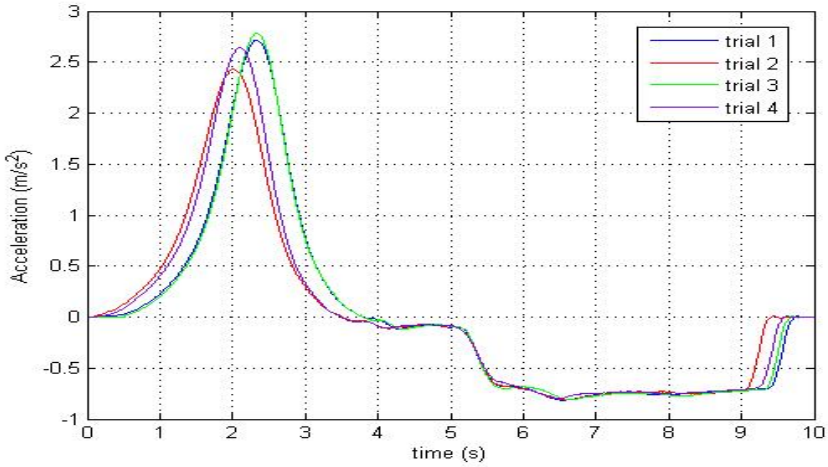

Figure 7.9. Accelerations calculated using Linear Encoder dataset, Case #1

Slip

Due to the application of the brake, slip (or creepage) occurred in the contact patch of the trailing wheelset (where brake was applied). The slip was measured as the difference between the longitudinal velocity (Fig. 7.8 (c)) and the circumferential velocity of the braked wheelset (Fig. 7.8. (b)). The occurrence of slip generated longitudinal retarding force that stopped the bogie. Fig 7.10 shows the difference between the longitudinal velocity and the circumferential velocity of the braked wheelset in the braking zone (from t=5s to t=10s). This figure *represents* the slip that occurred during the brake application.

With a view to obtaining slip through another data set (namely the velocity difference of the braked and unbraked wheelsets), the reference longitudinal velocity was set equal to the circumferential velocity of the unbraked leading wheelset. The slip calculated using this method is shown in Fig. 7.11. Both Fig. 7.10 and 7.11 show very good agreement. This finding has practical significance as it appears possible to

measure slip in the field without using the LIMES linear encoder system and purely through measurement of angular revolutions of the braked and unbraked wheelsets.

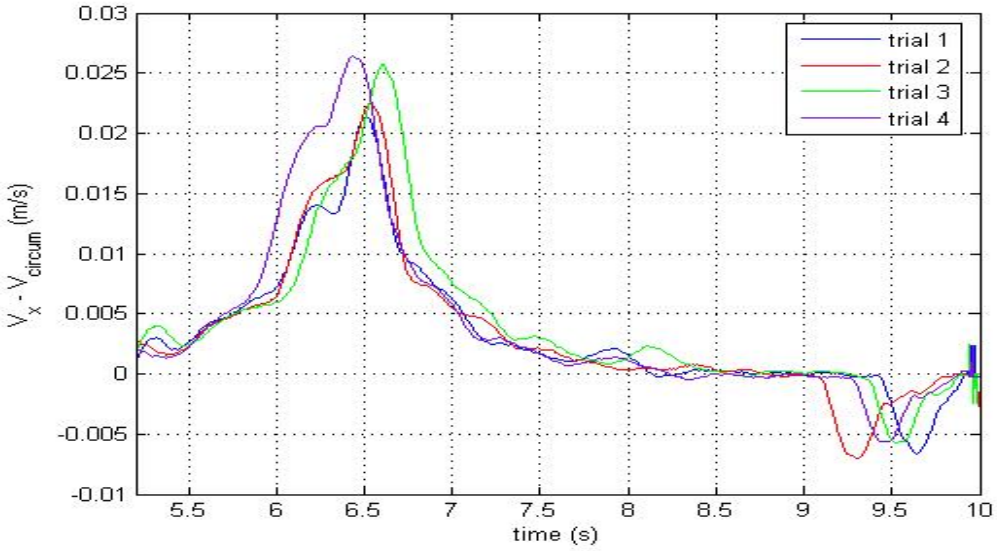

Figure 7.10 Difference between the longitudinal velocity (calculate from LIMES) and the circumferential velocity of the braked wheelset, Case #1

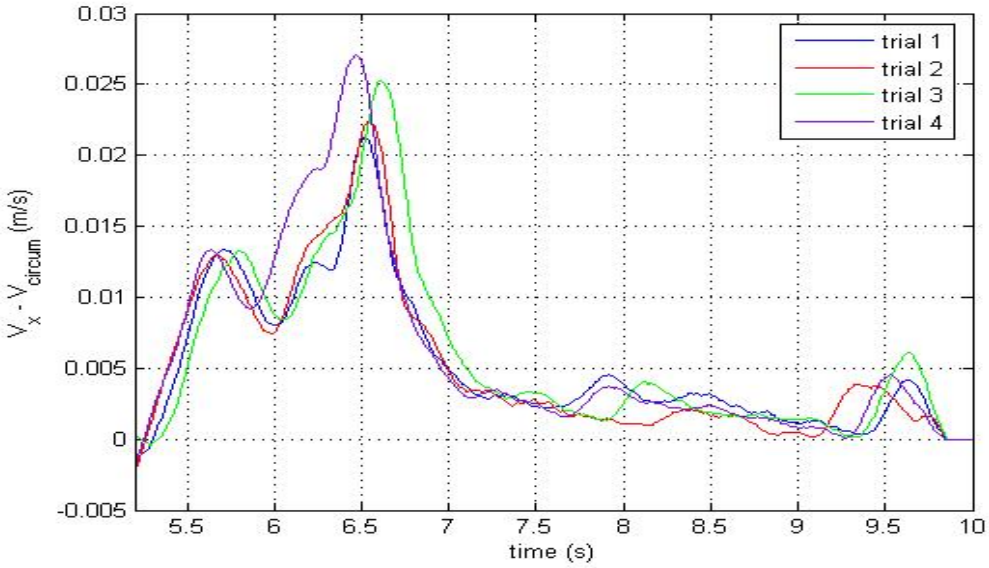

Figure 7.11. Difference between the longitudinal velocity (calculated from angular revolution of unbraked wheelset) and the circumferential velocity of the braked wheelset, Case #1

7.3. EXPERIMENT CASE #2 (P=150 KPA)

For the experiment Case #2, the brake pressure was increased to 150 kPa whilst maintaining the brake application time at 0.8 second. The brake force produced by 150 kPa cylinder pressure brought the braked trailing wheelset just into the skid limit. It was, therefore, difficult to predict whether skid would happen or not, as small changes to the system parameters, such as the friction coefficients and the dynamic wheel loads would have significant influence. Both the friction coefficient and the dynamic wheel load could easily change due to minor changes in the environmental and operational parameters.

7.3.1. Primary Data

Brake cylinder forces – normal and tangential

Fig 7.12 presents the brake cylinder pressure and forces measured in the brake rods of each cylinder for trials 1 to 4 during the execution of test Case #2. The figure shows that, when the brake was applied, the pressure in the brake cylinder increased from zero to 150 kPa in 0.8 second. The corresponding increase in the brake rod forces occurred without any time lag. Both rods measured approximately the same magnitude of brake shoe normal forces. The measured forces were approximately 19% lower than the force specified for new bogies (0.164 kN per kPa or 6.15 kN for 150 kPa) due to efficiency loss of the refurbished brake cylinder.

Fig. 7.13 shows the tangential brake force measured in the brake beam hanger for trials 1 to 4 of Case #2. As both the normal and the tangential brake shoe forces were measured, the friction coefficient between the brake shoe and the wheel tread (μ_s) was

able to be calculated, and the calculated values for Case #2 were found to vary between 0.23 and 0.30 (which compared favourably with Case #1 values of 0.27 - 0.33).

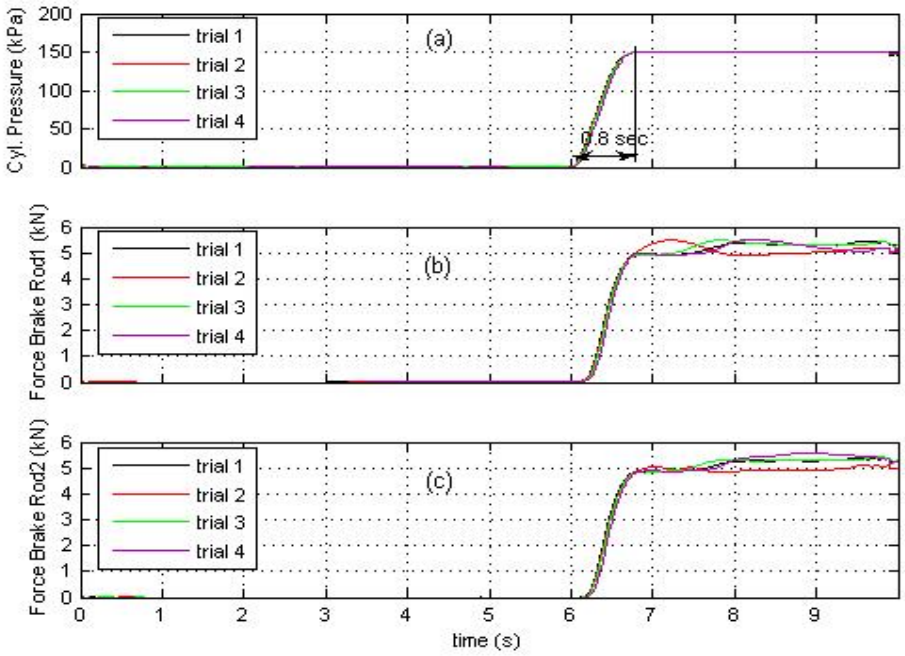

Figure 7.12. Brake cylinder pressure and forces in the brake rods, Case #2

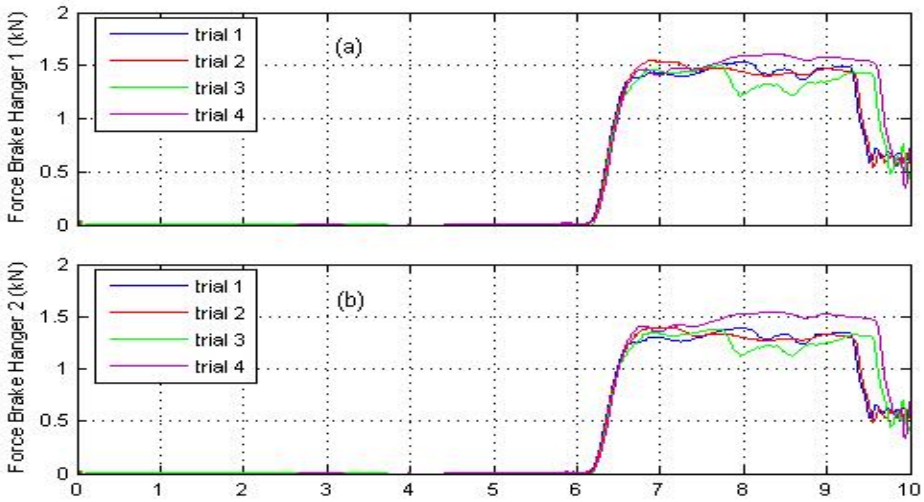

Figure 7.13. Tangential brake force in the brake beam hangers, Case #2

Accelerations

Fig. 7.14 shows the average of the measured longitudinal accelerations obtained from four accelerometers. The maximum longitudinal acceleration recorded varied from 1.8 m/s^2 to 2.4 m/s^2. Similar to the experiment Case #1, in the coasting zone each trial has provided a deceleration of approximately 0.1 m/s^2 due to rolling resistance. In the braking zone (the zone of interest of this test program) where the controlled brake was applied, the maximum deceleration obtained was 0.8 m/s^2 (trial 4).

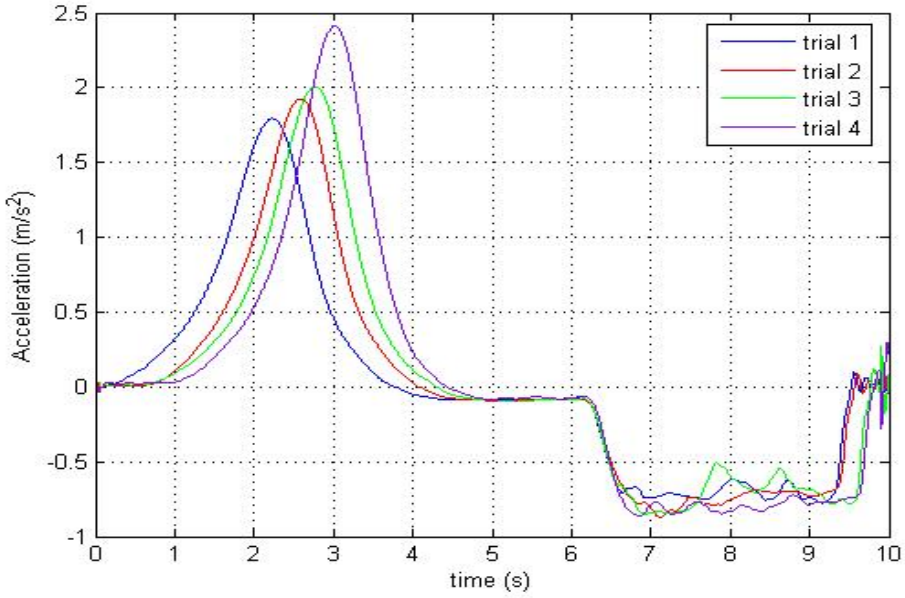

Figure 7.14. Accelerations measured by accelerometers, Case #2

Linear distance travelled and angular revolution of wheelsets

The travel distance of the bogie and rotation of the wheelsets during the experiment Case #2 is shown in Fig. 7.15. Fig. 7.15 (c) shows that the longest distance travelled has been 14.43 m. This distance related to the wheelset angular revolution of 36.25 rad, which was less than six full rotations of the wheelsets (see Fig. 7.15. (a) and (b)). The longest travel distance happened during the execution of the trial 4 when the highest

speed during the experiment Case #2 was achieved. When the skid occurred (trials 1 and 3), the angular revolution of the braked trailing wheelset was smaller than that of the unbraked leading wheelset.

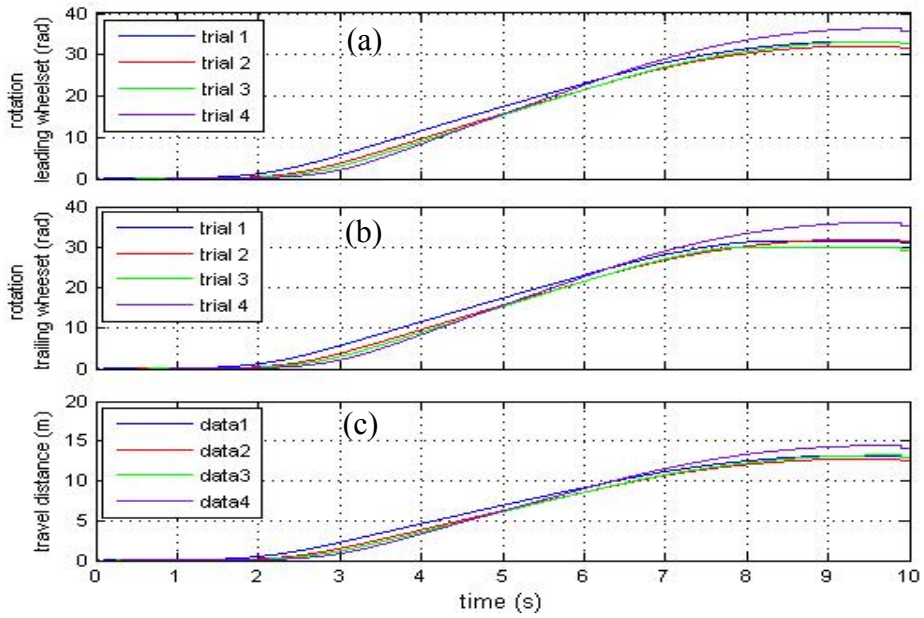

Figure 7.15. Travel distance and rotation of wheelsets, Case #2

7.3.2. Derived Data

7.3.2.1 Brake torque

Fig. 7.16 exhibits the brake torque applied to the trailing wheelset, calculated using Eq. 7.1. When severe skid happened (later discussion on Fig.7.17) the brake torque dropped drastically to 0.95 kN.m as shown in trial 3, whilst in the condition without skid the brake torque was as high as 1.25 kN.m. This result revealed that skid could adversely affect the braking performance of the bogie.

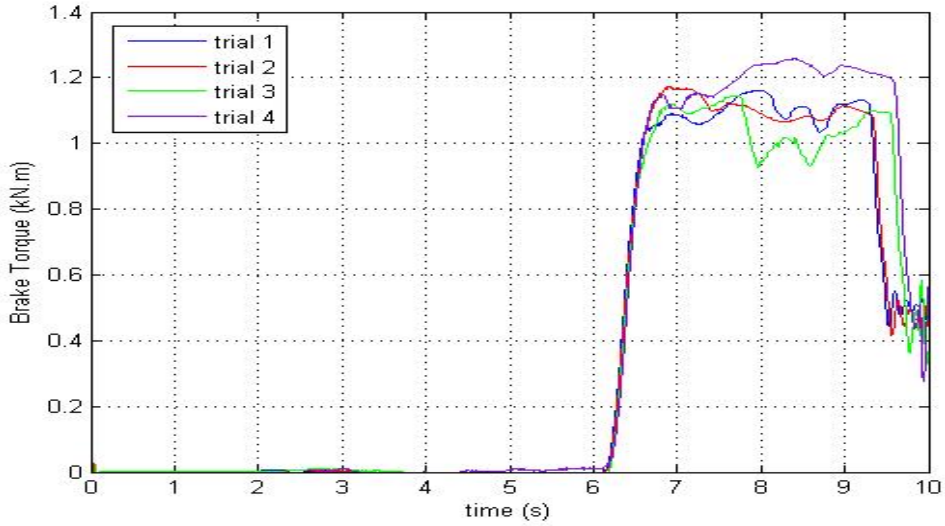

Figure 7.16. Brake torque applied to the trailing wheelset, Case #2

Speed profile and wheelsets angular velocity

The speed profile and the wheelset angular velocities of the bogie during the execution of the experiment Case #2 is presented in Fig. 7.17. The maximum speed obtained was 2.87 m/s (10.15 km/h), which occurred during trial 4. Fig. 7.17 (a) and (b) show that this speed is related to the wheelset angular velocity of 7.24 rad/s. Among the four trials of the experiment Case #2, wheelset skid occurred during trials 1 and 3 whilst in the other two trials wheelset skid did not occur. These results show that with the brake cylinder pressure of 150 kPa the braked wheelset was just on the verge of the onset of skid where the possibility to have skid is the same as the possibility of having no skid.

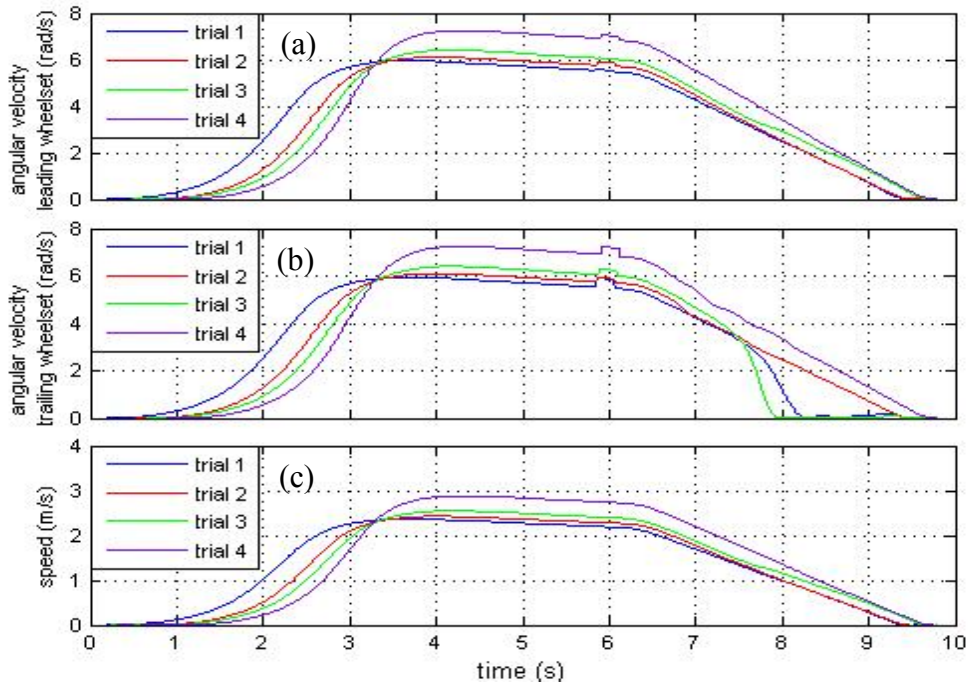

Figure 7.17. Speed profile and wheelsets angular velocity, Case #2

Longitudinal acceleration

Fig. 7.18 exhibits the bogie longitudinal acceleration time series obtained from the experiment Case #2 (calculated through the second order numerical differentiation of the linear distance data obtained from the LIMES linear encoder). Similar to the experiment Case #1, it provides a very good agreement with the direct measurement of longitudinal acceleration using accelerometers (Fig. 7.14). This shows that the onboard measurements are accurate enough and the wayside LIMES system provides an additional assurance on the accuracy of the onboard system measurements.

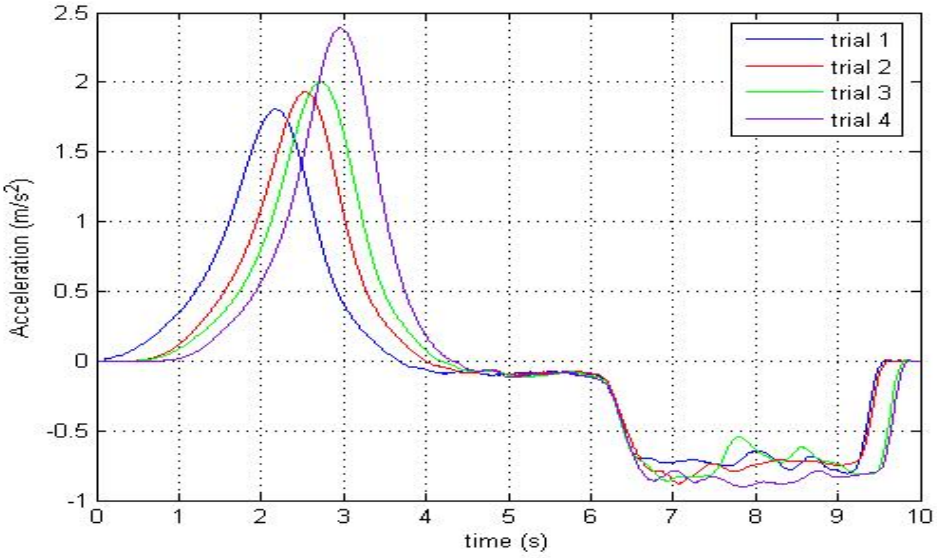

Figure 7.18. Accelerations calculated using Linear Encoder dataset, Case #2

Slip

Fig. 7.19 shows the difference between the longitudinal velocity and the circumferential velocity of the braked wheelset occurred during the application of the braking in Case #2. This figure represents the slip which occurred during the brake application. The longitudinal velocity used to obtain the curves in Fig. 7.19 was taken from the first derivative of the LIMES linear encoder dataset. For comparison, the slip was also calculated using the HENGSTLER shaft encoder of the unbraked wheelset as reference (Fig. 7.20). Both Fig. 7.19 and Fig. 7.20 show very good agreement. It can be clearly seen in Fig. 7.19 and Fig. 7.20 that, in trial 1, one hundred percent slip (skid) started to happen at t = 8.2 second as the circumferential velocity of the braked trailing wheelset becomes zero at this point of time. For trial 3, one hundred percent slip occurred earlier at t = 7.9 seconds.

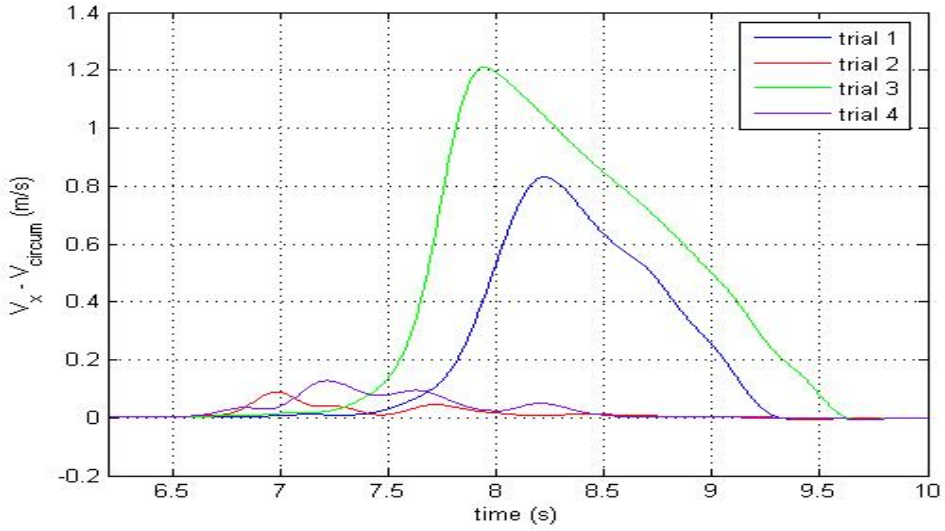

Figure 7.19. Difference between the longitudinal velocity (calculated from LIMES) and the circumferential velocity of the braked wheelset, Case #2

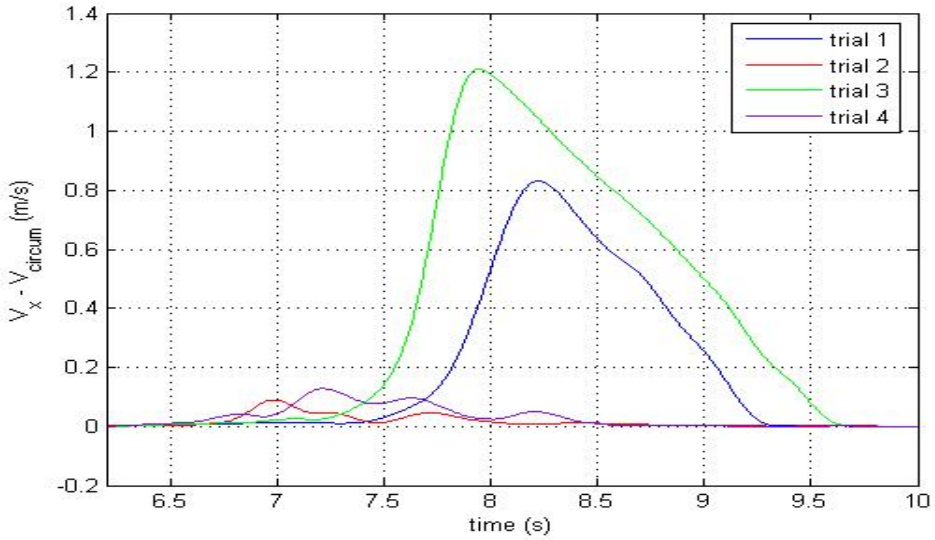

Figure 7.20. Difference between the longitudinal velocity (calculated from angular revolution of unbraked wheelset) and the circumferential velocity of the braked wheelset, Case #2

7.4. EXPERIMENT CASE #3 (P=180 KPA)

The purpose of the experiment Case #3 was to study the severe skid during the heavy braking. In the experiment Case #3 the brake pressure was increased to 180 kPa, much above the skid limit pressure. The brake application was maintained at 0.8 second. All trials exhibited skid of the braked wheelset. Results are presented below.

7.4.1. Primary data

Brake cylinder force – normal and tangential

Fig. 7.21 shows the brake cylinder pressure and forces measured in the brake rods of each cylinder for trials 1 to 4 during the execution of test Case #3. As can be seen in the figure, when the brake was applied the pressure in the brake cylinder increased from zero to 180 kPa in 0.8 second with the corresponding increase in the forces of the brake rods without any time lag. Both rods measured approximately the same magnitude of brake shoe normal forces. Similar to Case #1 and Case #2, the measured forces are slightly (approximately 15%) lower than that of the force specified for the new bogie (7.38 kN for 180 kPa) due to efficiency loss of the refurbished brake cylinder.

Fig. 7.22 shows the tangential brake force measured in the brake beam hanger for trials 1 to 4. As both the normal and the tangential brake shoe force were measured, the friction coefficient between brake shoe and wheel tread (μ_s) was able to be calculated. The calculated values for Case #3 varied between 0.21 and 0.28 (which compared favourably with Case #1 values of 0.27-0.33 and Case #2 values of 0.23-0.30)). It appears that with the increase in brake normal force, the friction coefficient reduces.

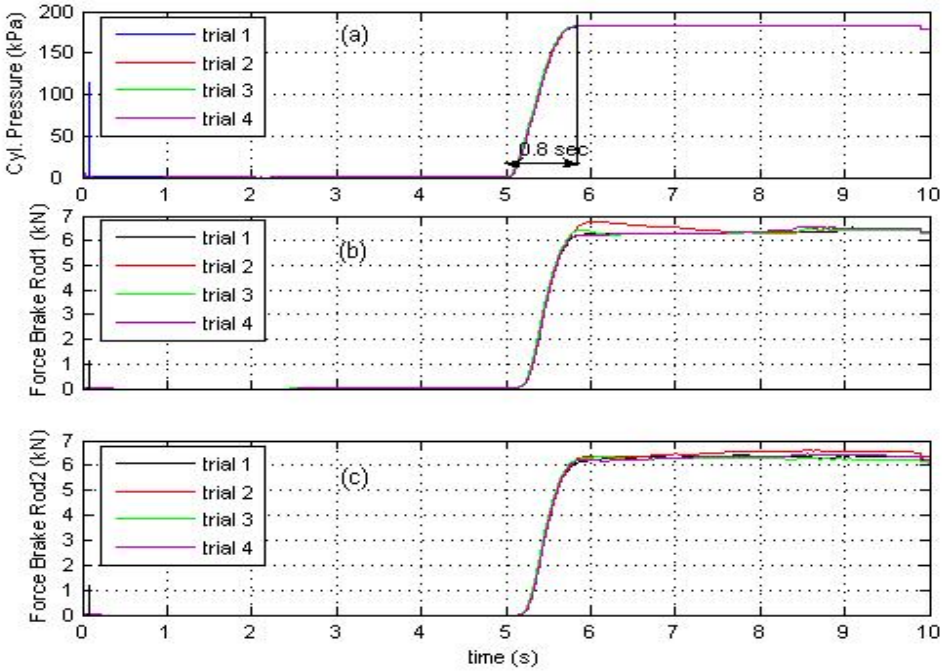

Figure 7.21. Brake cylinder pressure and forces in the brake rods, Case #3

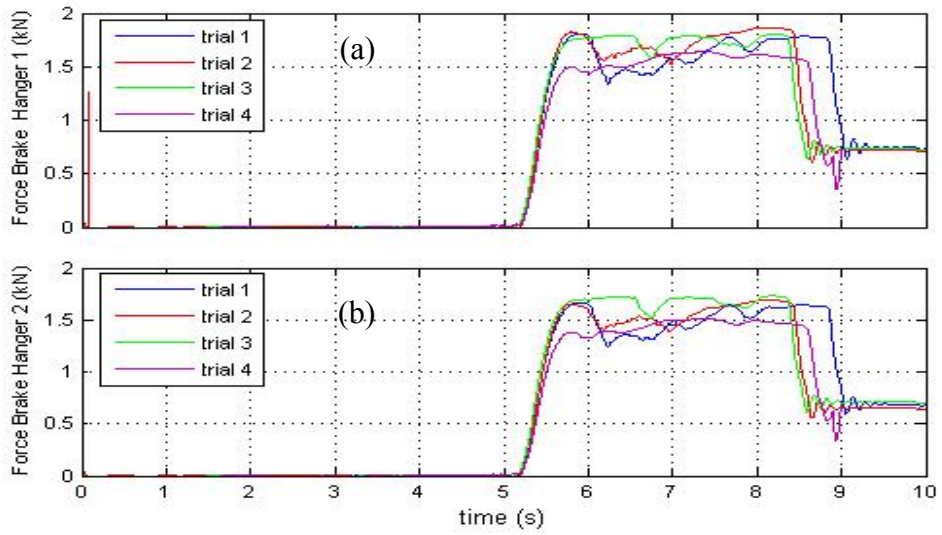

Figure 7.22. Tangential brake force in the brake beam hangers, Case #3

Accelerations

Fig. 7.23 shows the measured longitudinal acceleration of Case #3 (average value of four accelerometers). The maximum longitudinal acceleration recorded varied from 2.2 m/s^2 to 2.5 m/s^2. Similar to the experiments in Case #1 and Case #2, in the coasting zone each trial has provided a deceleration of approximately 0.1 m/s^2 due to rolling resistance. In the braking zone (the zone of interest of this test program) where the controlled brake was applied, the maximum deceleration recorded was 1.1 m/s^2 (trials 2 and 4). However, at the time of the severe skid (later discussion on Fig.7.26), the deceleration fell to 0.5 m/s^2 (trials 1 and 2).

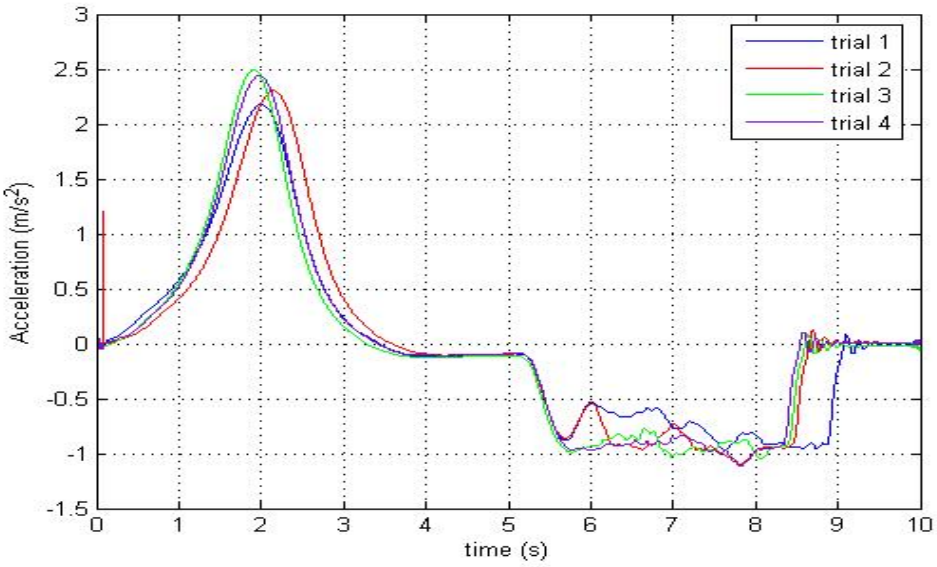

Figure 7.23. Acceleration measured by accelerometers, Case #3

Linear distance travelled and angular revolutions of wheelsets

Fig. 7.24 shows the angular revolution and the travel distance of the bogie obtained during Case #3. The maximum travel distance recorded was 16 m (Fig. 7.24 (c) – trial 1). Figs. 7.24 (a) and (b) reveal that for all trials the angular revolution of the braked

trailing wheelset was smaller than that of the unbraked leading wheelset due to skid (see Fig.7.26).

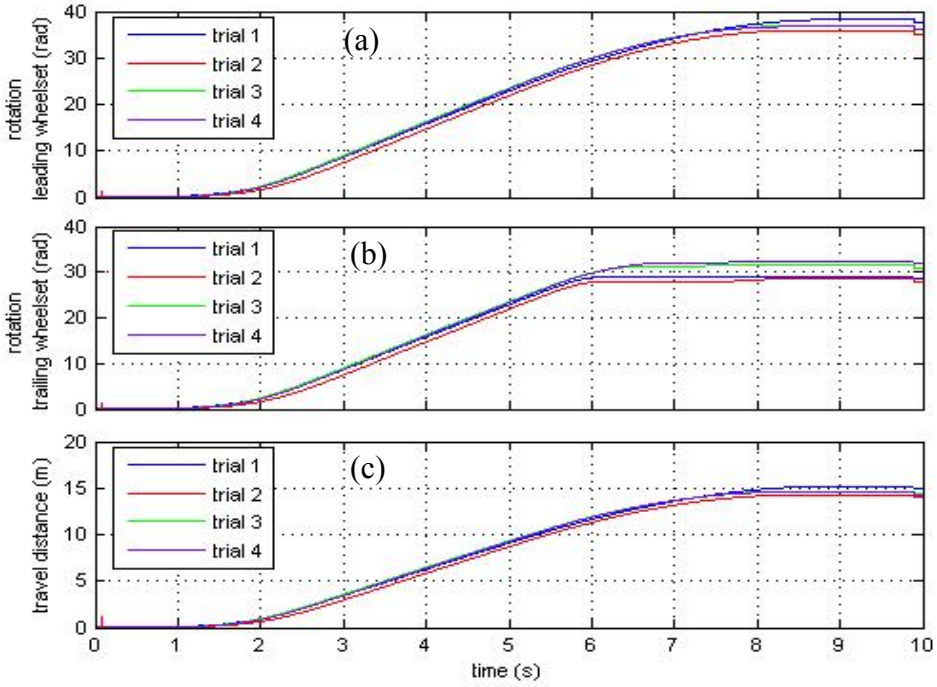

Figure 7.24. Travel distance and wheelsets rotation, Case #3

7.4.2. Derived Data

Brake torque

Fig. 7.25 shows the brake torque applied to the trailing wheelset during the experiment Case #3, calculated using Eq. 7.1. As expected, due to the skid of the trailing wheelset, the brake torque was found to drop drastically. As the most severe skid happened during trials 1 and 2 (see later discussion of Fig. 7.26), the most sudden decrease of the brake torque also occurred during these two trials. This result, again, shows that skid has significant negative effect on the braking performance.

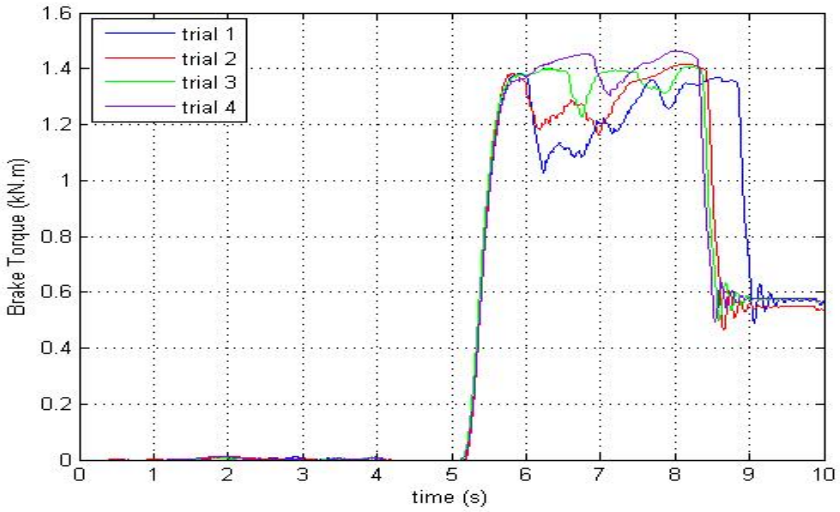

Figure 7.25. Brake torques applied to trailing wheelset, Case #3

Speed profile

Fig. 7.26 shows the speed profile and wheelset angular velocity during the experiment Case #3. As exhibited by Fig. 7.26, the rate of speed decrease was lower if the severe skid happened.

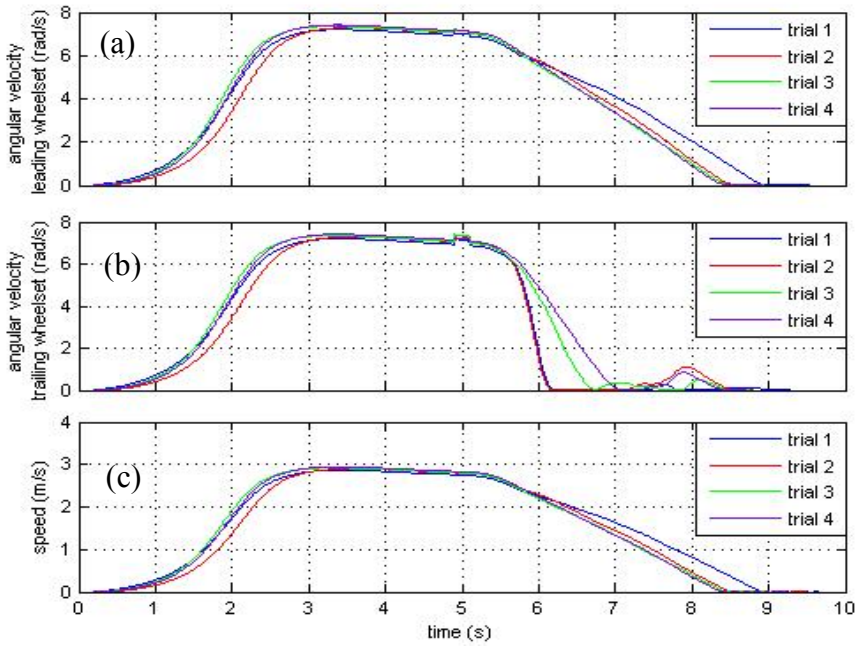

Figure 7.26. Speed profile and wheelsets angular velocity, Case #3

Longitudinal acceleration

Fig. 7.27 exhibits the bogie longitudinal acceleration time series obtained during the experiment Case #3, calculated through second order numerical differentiation of the linear distance data obtained from the LIMES linear encoder. Similar to the experiments in Case #1 and Case #2, it provides a very good agreement with the direct measurement of longitudinal acceleration using accelerometers (Fig. 7.23)

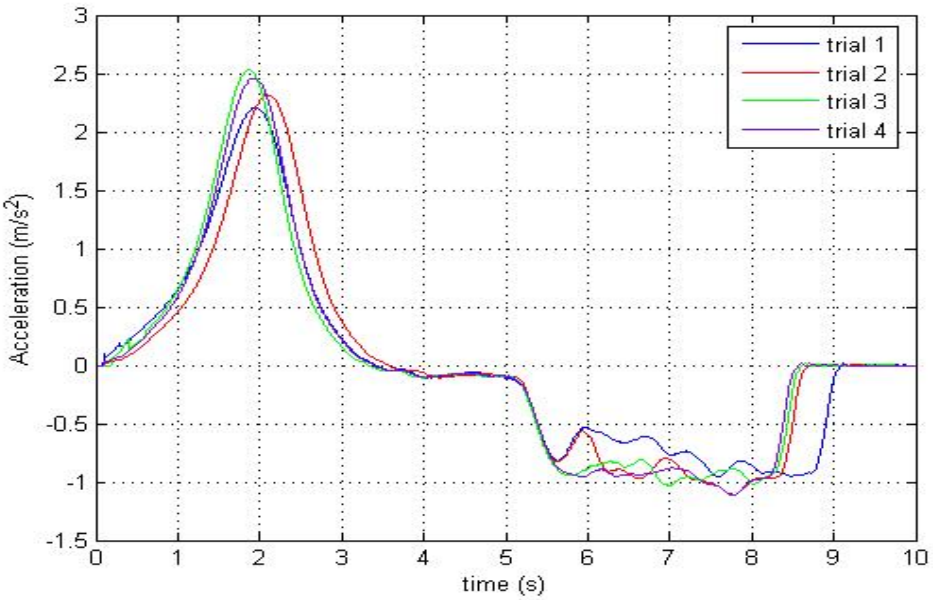

Figure 7.27. Longitudinal acceleration calculated from LIMES, Case 4

Slip

The slip that occurred during the brake application of Case #3 is shown in Fig. 7.28 and Fig. 7.29. The longitudinal velocity was used to obtain the curves in Fig. 7.28 whilst the angular revolution of the unbraked wheelset was used to obtain the curves in Fig. 7.29. Both Fig. 7.28 and Fig. 7.29 show very good agreement. Both figures show one hundred percent slip during all four trials of Case #3. For trials 1 and 2 the skid was detected at around 2.2 m/s, and for trials 3 and 4 it was detected at lower speeds of 1.65 m/s and 1.35 m/s respectively.

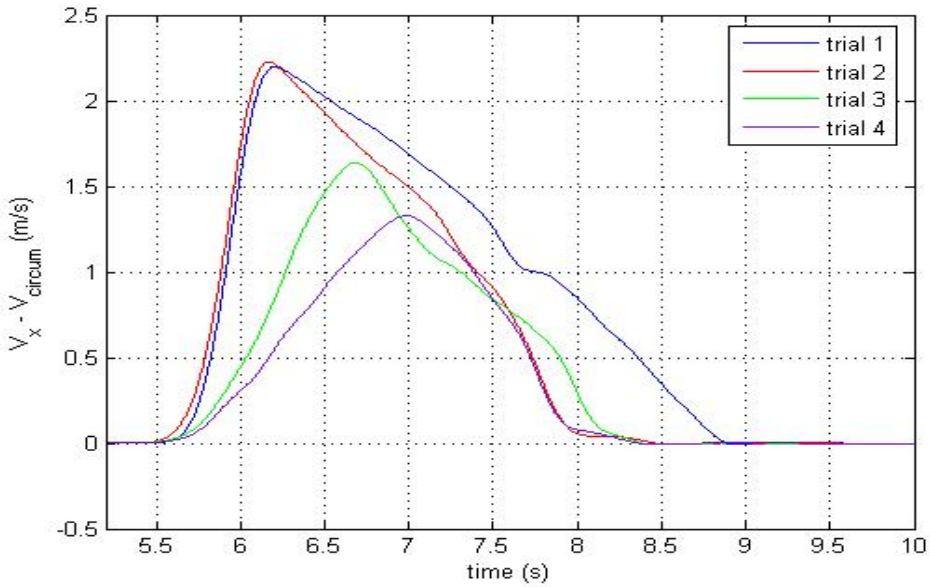

Figure 7.28. Difference between the longitudinal velocity (calculated from LIMES) and the circumferential velocity of the braked wheelset, Case #3

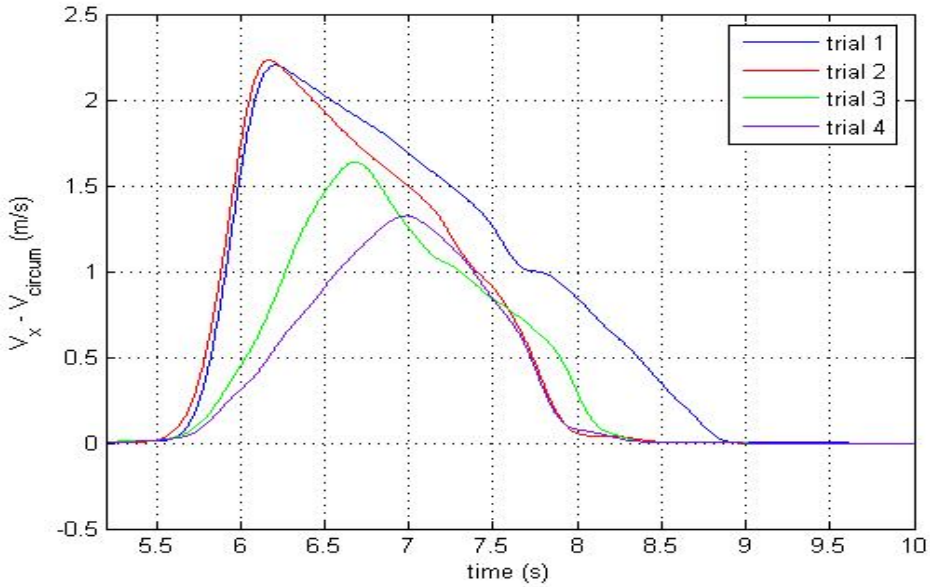

Figure 7.29.Difference between the longitudinal velocity (calculated from angular revolution of unbraked wheelset) and the circumferential velocity of the braked wheelset, Case #3

Friction coefficient between the wheel and the rail

When skid occurs the following equation is fulfilled:

$$T_B = (\mu_{r1} N_{w1} r_{w1}) + (\mu_{r2} N_{w2} r_{w2}) \quad (7.2)$$

where T_B is the brake torque applied to the wheelset (see Eq. (7.1)), μ_{r1} and μ_{r2} are the friction coefficients at the right and the left wheel-rail contact patches respectively, N_{w1} and N_{w2} are the normal loads on the right and the left wheel-rail contact patches respectively and r_{w1} and r_{w2} are the rolling radius of the right and the left wheels respectively. Assuming $\mu_{r1} \approx \mu_{r2} = \mu_r$ and rolling radius of the wheels $r_{w1} \approx r_{w2} = r_w$, Eq. (7.2) can be written as

$$T_B = \mu_r r_w (N_{w1} + N_{w2}) \quad (7.3)$$

During the experiments T_B was obtained by measuring the tangential brake force whilst the nominal wheel radius r_w=0.398m, measured prior to the test execution and N_{w1} and N_{w2} were the right and the left wheel load (sum of the components due to static load and bogie pitching dynamics) of the braked wheelset respectively ($N_{w1} \approx N_{w2} \approx 8.85kN$). Therefore, when skid happened, the friction coefficient between wheel and rail, μ_r, was calculated using Eq. (7.3).

The calculated friction coefficient between the wheel and the rail during the occurrence of skid in this experiment program was found to vary between 0.15 and 0.20. The low coefficient is believed to be typical of "rough" running surfaces; as the running surfaces were not polished to any precision and patches of corrosion products were visible to the naked eye, especially on the railhead, the low friction was considered acceptable.

The friction coefficient calculated from the skid measurements was much lower than the value obtained from the tribometer measurement (0.50 - 0.55 for dry rail and 0.43 - 0.46 if soapy water was applied to the rail surface; see Appendix II). As tribometer measurements could not be regarded as an accurate reflection of the actual case (due to speed /wheel profile /wheel material, for example), the measured tribometer values were disregarded. Field practice also agrees with this decision as tribometer values are only used to determine *relative* changes to the friction coefficients rather than for the *absolute* measure. The friction coefficient calculated from Eq. (7.3) was therefore incorporated in the simulation of the experimental cases reported in Chapter 8.

7.5. SUMMARY AND CONCLUSION

The results of the experimental program described in Chapter 6 have been presented in this chapter. All measurement devices (both onboard and wayside) worked well giving accurate results resulting in good inter-dependent comparisons. All the data gathered from the measurements were found to be consistent. Three cases of experiments were selected for the purpose of reporting. The only variable between the three cases was the brake pressure (130kPa, 150kPa and 180kPa) with the brake application time being kept constant (0.8 sec) for all cases.

From the results of the experiments some important conclusions can be drawn as listed below:

- The piston forces exerted by the brake cylinder (force measured in brake rod) were found to be approximately 15% to 20% lower than the value calculated from the bogie specification at its new condition indicating reduction of the efficiency of the refurbished bogie brake system compared to the new one.

- At the brake pressure of 130 kPa there was no skid detected, showing that at this pressure the bogie was braked below its skid limit.

- At the brake pressure of 150 kPa the braked trailing wheelset was brought into the skid limit region. Within this region the possibility of encountering skid was the same as the possibility of not encountering skid. This uncertainty is due to small changes in the system parameters, such as the friction coefficients and the dynamic wheel loads, would have significant influence.

- The acceleration signatures obtained from direct measurement using the accelerometers agree very well with the acceleration signatures calculated from the second order numerical difference of the LIMES linear encoder data set.

- At the brake pressure of 180 kPa, wheelset skid was detected for all the four trials, showing that at this pressure the bogie was braked above its skid limit.

- Both slip calculation using LIMES linear encoder and using non-braked wheelset shaft encoder as reference to calculate longitudinal velocity showed very good agreement. This finding leads to potential field measurement of slip without the LIMES linear encoder.

- From the measurement of the normal and tangential brake shoe forces, friction coefficients between the brake shoe and the wheel tread were calculated for all cases. It appeared that with the increase in brake shoe forces (or brake cylinder pressure), the coefficient of friction between the brake shoe and the wheel tread reduces. For the 130kPa, 150kPa and 180kPa cylinder pressures, the average friction coefficients determined were 0.30, 0.27 and 0.25 respectively.

- From the six skid trials reported in this chapter, the friction coefficient between the wheel tread and railhead was determined and was found to vary between 0.15 – 0.20. This range is much smaller than the coefficients determined from the tribometer readings (0.50 – 0.55). As the tribometer is considered more relevant for understanding relative changes in friction coefficient, the absolute values of friction coefficient obtained from the tribometer measurements were disregarded. More reliable determination of friction coefficient between the wheel tread and railhead is therefore considered to be the one obtained through the skid trials (0.15 – 0.20).

- The results of the experiment were found to be ***consistent and reliable***; thus they can be used to validate the RBD program built by the author. The validation is reported in Chapter 8.